Mass and Energy Transports in an Undisturbed Atlantic Trade-Wind Flow

ERNST AUGSTEIN—*Institute für Radiometeorologie und Maritime Meteorologie an der Universität Hamburg, Germany*

HERBERT RIEHL [1]—*Department of Atmospheric Science, Colorado State Univervity, Fort Collins, Colo.*

FEODOR OSTAPOFF—*Sea–Air Interaction Laboratory, Environmental Research Laboratories, NOAA, Miami, Fla.*

VOLKER WAGNER—*Institut für Radiometorologie und Maritime Meteorologie an der Universität Hamburg, Germany*

ABSTRACT—The vertical and horizontal mass and energy transports for the layer between the sea surface and 700 mb are calculated for the first (undisturbed) period of the Atlantic Trade-Wind Experiment 1969. The trade-wind inversion represents a layer with a strong downward mass flux due to the mean motion. The height of the inversion and its thermodynamic properties seem to depend on the balance between the mean atmospheric sinking and the turbulent mixing.

Because of the vertical transport from the sea surface into the atmosphere, this process assures that water vapor is totally accumulated in the layer below the inversion and transported downstream into the equatorial trough region. Thus the effectiveness of the atmospheric heat absorption in the trades as a force for driving the large-scale circulation is closely related to the vertical static structure as well as to the kinematic field of the low-level trade-wind region.

1. INTRODUCTION

Studies by v. Ficker (1936) and Riehl et al. (1951) have shown that the low-level trade-wind regime over the oceans plays an important role in the atmospheric energy cycle. Further investigations, such as those by Riehl and Malkus (1957), Malkus (1958), Aspliden (1971) and Augstein (1972) have confirmed that there is a net gain of energy in the atmosphere between the sea surface and the trade-wind inversion. Malkus (1958) emphasized that the heating mechanism of the trade-wind circulation is determined by a complex interaction between microscale processes near the sea surface, meso-scale convection, and large-scale horizontal transports. This concept of scale interaction has drawn increasing attention during the last decade (Garstang 1972). Progress must depend, in part, upon investigations of the mass, heat, and water vapor fluxes in the entire planetary boundary layer in terms of different levels of atmospheric organization. This study concentrates on the turbulent and mean motion transports in the lower layers of the Atlantic trade-wind flow under relatively undisturbed conditions.

2. THE ATLANTIC TRADE-WIND EXPERIMENT (ATEX)

ATEX was conducted during February 1969 in the Atlantic Northeast trade-wind region. During this experiment, an intensive aerological program, concentrated in the lowest 4000 m of the atmosphere, was carried out from three ships (R.V. *Meteor*, R.V. *Planet*, and R.V. *Discoverer*). In the first period of the experiment, a fourth ship, HMS *Hydra*, also participated. *Meteor*, *Planet*, and *Discoverer* formed the corners of an equilateral triangle with sides of about 750 km. This ship array drifted for nearly 3 weeks in a well-developed trade-wind flow. The center of the triangle moved from 13.5°N, 34.7°W on February 6 to 9.5°N, 40.6°W on February 22 (fig. 1). The objectives of the program and details of the measurements are described by Brocks (1972).

Radiosonde and radar wind observations were obtained at the corners of the triangles imultaneously at 3-hr. intervals. Radiosonde releases without wind measurements were made from HMS *Hydra*. In addition to routine deck-level observations (temperature, humidity, wind velocity, cloudiness, etc.), which were carried out at least every 90 min, the turbulent surface fluxes were measured from buoys near *Meteor* and *Planet* by the profile method and the eddy correlation technique. The buoy data were also used as reference values to correct the ship's deck-level measurements for effects caused by the ship's environment.

It is important to note that the ships assembled on three separate occasions for the purpose of intercomparison and calibration. *Hydra* and *Meteor* had two test series of several hours, the first at the beginning of the drift and the second when *Hydra* left the array 14 days later. *Meteor*, *Planet*, and *Discoverer* met for a 1-day intercomparison at the end of the experiment. This com-

[1] Now at the Institut für Meteorologie, Freie Universität Berlin, Germany
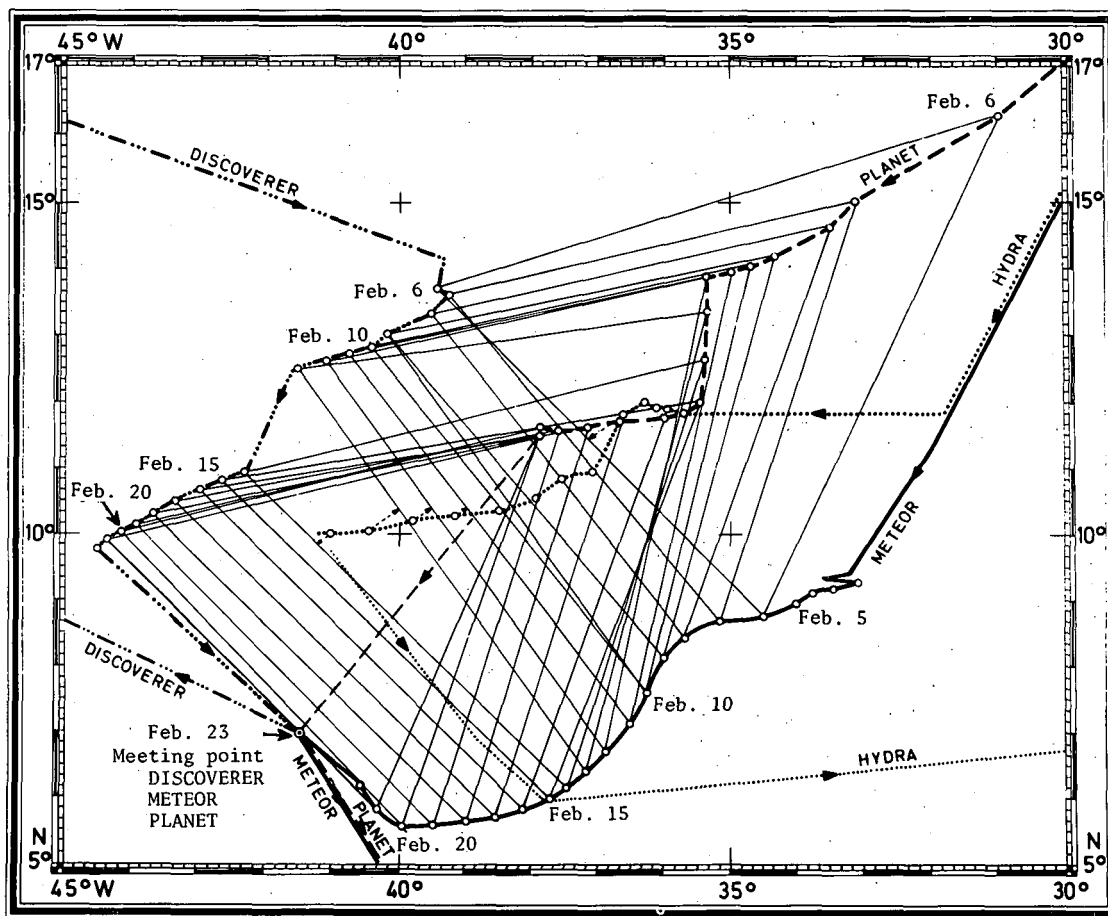
FIGURE 1.—Successive positions of the ATEX triangle Feb. 6–21, 1969. The thin, solid lines show the boundaries of the triangular base for each day.
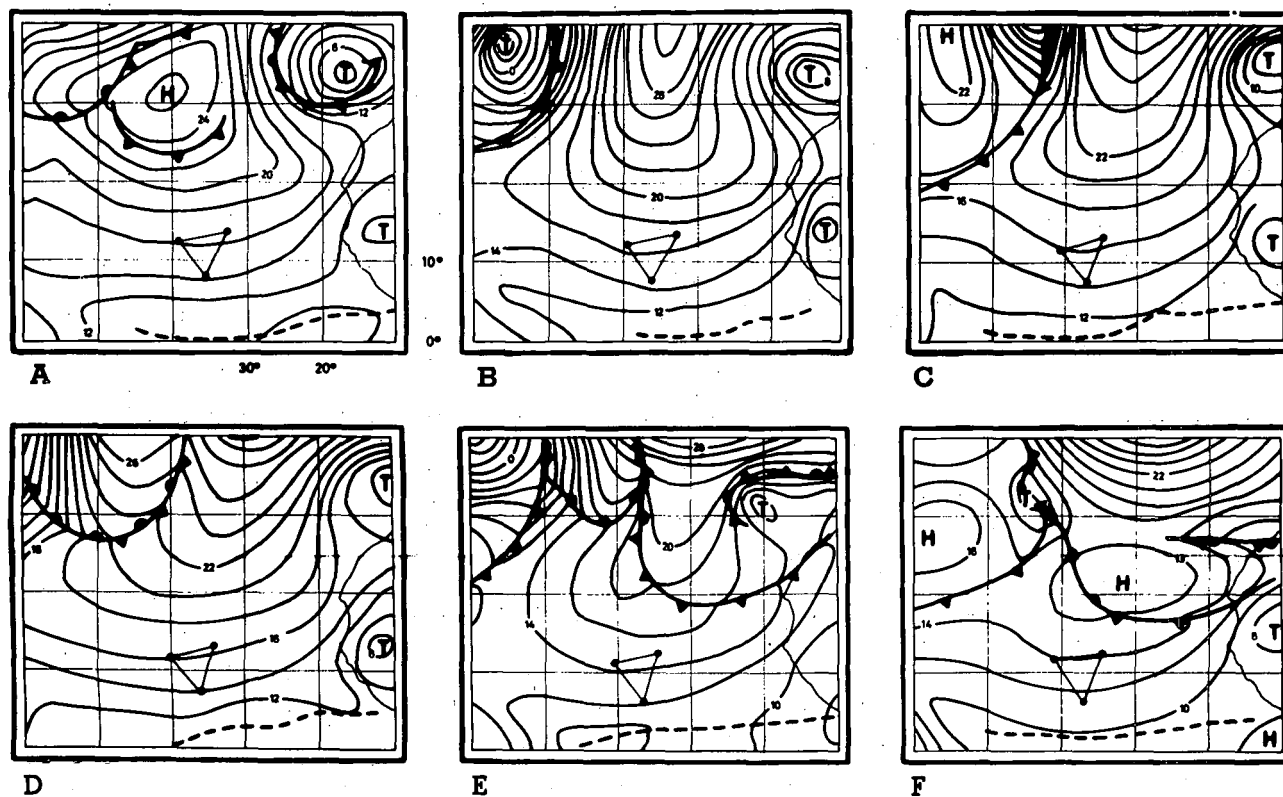

FIGURE 2.—Surface isobars (mb, last two digits only) for (A) Feb. 7, (B) Feb. 8, (C) Feb. 9, (D) Feb. 10, (E) Feb. 11, and (F) Feb. 12, 1969. ATEX triangle is indicated for each day. Conventional frontal symbols and dashed line for equatorial low-pressure trough have been entered.
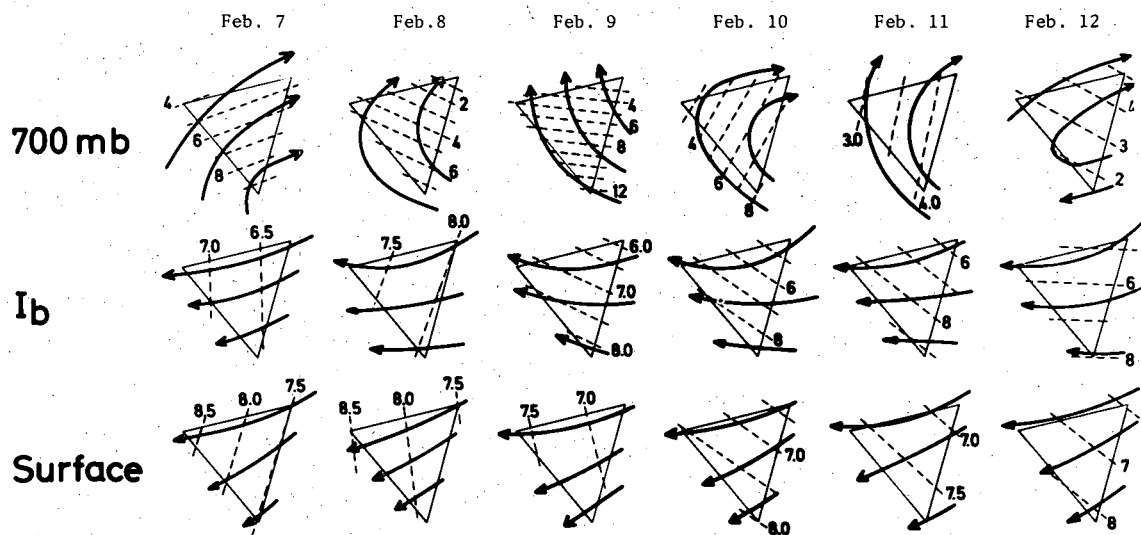
FIGURE 3.—Streamlines (solid) and isotachs (m/s, dashed) for surface, inversion base (I_b), and 700-mb level in the area of the ATEX triangle, Feb. 7–12, 1969.

parison showed substantial differences in the deck-level pressure and temperature readings of the three ships. These deck-level measurements are also used as baseline values for the radiosondes. Corrections based upon the intercalibration test were applied in the subsequent data reduction. The details of the procedures are discussed by Augstein et al. (1973) and Brümmer et al. (1973). Finally, simultaneously tracked balloon targets showed that the statistical noise of the three radars was different. Therefore, filtering methods were applied to achieve compatibility of soundings (Brümmer et al. 1973).

3. THE SYNOPTIC SITUATION

The observational period may be roughly subdivided into two parts. The first period (February 7–12), discussed in this paper, was governed by a well-developed northeast trade-wind flow. Convective activity was weak or absent in the entire area and the trade inversion could be detected in all radiosonde soundings.

The surface pressure field in figure 2, analyzed by Soltwisch (1973), demonstrates that the triangle was embedded in a nearly classical trade-wind situation. The steadiness of the wind field below the inversion may be seen from figure 3. The daily averaged streamline field between the sea surface and the inversion base hardly changed during this period. Air in this layer is always accelerated due to flow toward lower pressure. Contrary to the steady regime in the moist layer below the inversion, strong differences exist from day to day in the wind field above the inversion. These differences are illustrated on the 700-mb charts. The horizontal flow below and above the inversion appeared to be decoupled. This conclusion can also be drawn from the mean wind profile of the triangle in figure 4. While the lower layers were marked by a small standard deviation, time variations increased above the inversion. This is especially true for wind direction. Figure 4 also shows strongest wind speeds in the layer below cloud base. The directional shear was
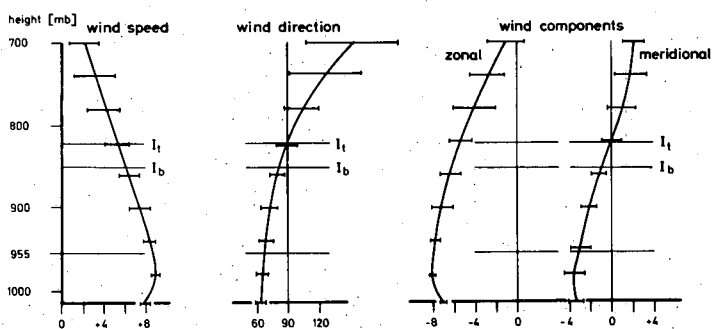

FIGURE 4.—Vertical profiles of wind speed (m/s) and wind direction (deg.) applicable at the center of the ATEX triangle and averaged over the period, Feb. 7–12, 1969. Bars indicate standard deviation and I_b and I_t denote inversion base and top, where the averaging has been performed with respect to the variable positions of the inversion in space and time.
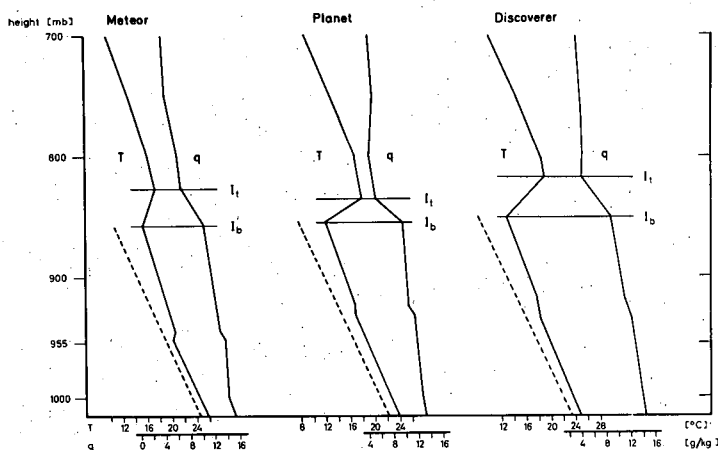

FIGURE 5.—Vertical profiles of temperature, T, and specific humidity, q, averaged as indicated in figure 4. Dashed line denotes dry-adiabatic lapse rate.

small below the inversion (1°/10 mb) but increased rapidly in the upper layer (7°/10 mb).

The averaged temperature and humidity profiles in figure 5, obtained by a smoothing technique that preserves

the layered trade-wind structure, are in good agreement with measurements of Bunker et al. (1950) and Augstein (1972) in other regions of the Atlantic trade-wind zone. At all ATEX positions, the temperature gradient in the lowest 500 m was almost dry adiabatic and the specific humidity nearly constant with height. The transition zone, characterized by a stable temperature distribution and strong water vapor decrease with height, that generally tops the mixed layer was not always present. This was especially true at the upstream position of *Planet* where it was found in only about 60 percent of the soundings. The inversion was stronger at *Planet* and *Discoverer* and weaker at *Meteor*, which was situated closest to the equatorial trough region (ETR). During the period under dicussion, no precipitation was observed on *Planet* and *Discoverer;* only a few small showers were registered in the vicinity of *Meteor.* This fact justifies the assumption that no serious error is introduced if net condensation heating is neglected in the subsequent energy budget calculations.

4. THE ANALYSIS PROCEDURE

The Vertical Scale Subdivision and Averaging Procedures

Following earlier studies, we have divided the layer between the sea surface and 700-mb level into four sublayers. The lowest one, the subcloud layer, is arbitrarily assigned a thickness of 60 mb, which is approximately supported by observations. Hence, the 955-mb level was taken as its upper boundary. The next layer, extending from 955 mb to the inversion base, is nearly identical with the cloud layer where trade-wind cumuli are usually found. Both the cloud layer and the overlying layer, which was defined by the top and the bottom of the inversion, were subject to much variation. Finally, the top layer is taken from the inversion top to the 700-mb level. Such a vertical subdivision (fig. 5) provides a framework within which we might gain some insight into the interrelation between the horizontal and vertical mass and energy transports and the respective layers of the trade-wind atmosphere. Statistical instrumental errors and small-scale turbulence are smoothed out by averaging each layer in the vertical and in time over 1 day (normally eight soundings). The time scale is also compatible with the scale size of the triangle in view of the mean wind speed.

The Budget Computations

The derivation of the energy equation based on the first law of thermodynamics and the equation of continuity is well known. Referring to unit mass we find

$$\frac{\partial}{\partial t} \rho\left(\frac{v^2}{2}+gz+c_vT\right)=-\text{div}\left[\rho\mathbf{V}\left(\frac{v^2}{2}+gz+c_pT\right)\right.$$
$$\left.-F\mathbf{V}+\mathbf{R}+\mathbf{C}\right] \quad (1)$$

where $\partial/\partial t$ is the local derivative, ρ is air density, $\mathbf{V}$ is the three-dimensional wind velocity, g is the acceleration of gravity, z is the vertical coordinate, c_v is specific heat at

constant volume, c_p is specific heat at constant pressure, T is temperature, div is the three-dimensional divergence, F is frictional stress, $\mathbf{R}$ is the heat flux due to total radiation, $\mathbf{C}$ is the heat flux due to molecular heat conduction, c_pT is enthalpy, and c_vT is internal energy.

In the following, we will consider kinetic energy, $v^2/2$, frictional force, F, and heat conduction, $\mathbf{C}$ to be small compared to the other terms, assumptions that are supported by the observations.

Integrating eq (1) over a volume V and applying Gauss' theorem to the terms with geopotential energy and enthalpy, one obtains

$$\int_V \frac{\partial}{\partial t}\rho(gz+c_vT)dV=-\int_S \rho\mathbf{V}(gz+c_pT)\cdot\mathbf{n}\,dS$$
$$-\int_V\text{div}\,\mathbf{R}\,dV \quad (2)$$

where S is the surface of the volume V, $\mathbf{n}=(\mathbf{i}n_x+\mathbf{j}n_y+\mathbf{k}n_z)$ is the vector normal to the surface S and $\mathbf{i}$, $\mathbf{j}$, $\mathbf{k}$ are unit vectors of a Cartesian system.

Separating horizontal and vertical components of the first term on the right side of eq (2) and allowing the top and the bottom of the volume to have a slope with respect to the earth's surface, we get

$$\int_V \frac{\partial}{\partial t}\rho(gz+c_vT)dV=-\int_H \rho v(gz+c_pT)n_{xy}dH \quad (3a)$$
$$-\int_{F_t} \rho v(gz+c_pT)n_{xy}dF \quad (3b)$$
$$+\int_{F_b} \rho v(gz+c_pT)n_{xy}dF \quad (3c)$$
$$-\int_{F_t} \rho w(gz+c_pT)n_zdF \quad (3d)$$
$$+\int_{F_b} \rho w(gz+c_pT)n_zdF \quad (3e)$$
$$-\int_V \text{div}\,\mathbf{R}\,dV \quad (3f)$$

where n_{xy} is the horizontal component of the normal vector, n_z is the vertical component of the normal vector, H is the area of the vertical surface of the volume, F_t is the surface of the top of the volume, F_b is the surface of the bottom of the volume, v is the horizontal wind component, and w is the vertical wind component.

The terms on the right side of eq (3) have the following meaning:
  (3a) Horizontal flux through H.
  (3b) Horizontal flux through F_t. ⎫ (due to the slope of
  (3c) Horizontal flux through F_b. ⎭ the boundaries)
  (3d) Vertical flux through F_t.
  (3e) Vertical flux through F_b.
  (3f) Divergence of $\mathbf{R}$ in the specified volume.

The terms (3b) and (3c) refer to the flux through the top and the bottom of the volume established by the horizontal wind component. Therefore, if F_t and F_b are parallel to the earth's surface, terms (3b) and (3c) become zero. The equation for the water vapor budget correspond-

ing to eq (3) is expressed by

$$L\int_V \frac{\partial}{\partial t}(\rho q)dV = -L\int_H \rho v q n_{xy}dH \qquad (4a)$$

$$-L\int_{F_t}\rho v q n_{xy}dF \qquad (4b)$$

$$+L\int_{F_b}\rho v q n_{xy}dF \qquad (4c)$$

$$-L\int_{F_t}\rho w q n_z dF \qquad (4d)$$

$$+L\int_{F_b}\rho w q n_z dF \qquad (4e)$$

$$-L\int_V (q_c-q_E)dV \qquad (4f)$$

where q is specific humidity, L is latent heat of vaporization of water, q_c is the water vapor condensed in the volume V, and q_E is the evaporated water in the volume V.

The terms (4a)–(4e) represent the water vapor fluxes in the same way as enthalpy and geopotential energy fluxes are described in terms (3a)–(3e). Term (4f) represents the difference between water vapor loss by condensation and water vapor gain by evaporation within the volume. As already mentioned, however, virtually no precipitation was observed during the period, and there was little change in low-level cloudiness at all stations. Therefore, the last term of eq (4) can be neglected.

To consider mean and turbulent processes separately, we must distinguish between grid and subgrid transports. We therefore use the following notation for a property X:

$$X=\bar{X}+X' \text{ and } X=\tilde{X}+X^*$$

with

$$\bar{X}=\frac{1}{\Delta p}\int_p X dp \qquad \text{(vertical average)}$$

and

$$\tilde{X}=\frac{1}{F}\int_F X dF. \quad \text{(surface average over } F, \text{ which can be the top and bottom of the volume)}$$

Asterisked or primed quantities indicate the local deviations from the averages. Furthermore, we assume that the divergence of horizontal subgrid fluxes is small compared to the other terms and can be neglected. Finally, the terms (3a) and (4a) are, in practice, computed by averaging the vertically integrated properties along the connecting lines l_i between the ships. This average is marked by the double bar in eq (5) and (6). This procedure also implies linear changes of the mass flux as well as of other meteorological values. *Hydra*, lying approximately midway between the *Meteor* and the *Discoverer*, provided a partial check on the assumption of linearity, at least in the lower layers. No strong departures from linearity were observed in the data obtained by *Hydra*. Applying the above notation and additional assumptions to eq (3) and (4), we obtain eq

(5) for heat and geopotential energy and (6) for latent heat transports; that is,

$$\int_V \frac{\partial}{\partial t}\rho(c_v T+gz)dV$$

$$=\frac{1}{g}\sum_{i=1}^3 \overline{\overline{(\overline{c_p T}+\overline{gz})\bar{v}n_{xy}\overline{\Delta p}}}_i l_i$$

$$-[(c_p\tilde{T}+\tilde{gz})_{top}\widetilde{\rho v}_{top}n_{xy}F_{top}$$

$$-(c_p\tilde{T}+\tilde{gz})_{bot}\widetilde{\rho v}_{bot}n_{xy}F_{bot}]$$

$$-[(\widetilde{\rho w})_{top}(c_p\tilde{T}+\tilde{gz})_{top}n_z F_{top}$$

$$-(\widetilde{\rho w})_{bot}(c_p\tilde{T}+\tilde{gz})_{bot}n_z F_{bot}]$$

$$-[c_p\widetilde{(\rho w)^*_{top}T^*_{top}}n_z F_{top}-c_p\widetilde{(\rho w)^*_{bot}T^*_{bot}}n_z F_{bot}]$$

$$-\int_V \text{div }\mathbf{R}\,dV \qquad (5)$$

and

$$L\int_V \frac{\partial}{\partial t}(\rho q)dV=\frac{1}{g}\sum_{i=1}^3 \overline{\overline{(L\bar{q}\bar{v}n_{xy}\overline{\Delta p})}}_i l_i$$

$$-L[(\widetilde{\rho q}_{top}\tilde{v}_{top}n_{xy}F_{top})-(\widetilde{\rho q}_{bot}\tilde{v}_{bot}n_z F_{bot})]$$

$$-L[(\widetilde{\rho w})_{top}\tilde{q}_{top}n_z F_{top}-(\widetilde{\rho w})_{bot}\tilde{q}_{bot}n_z F_{bot}]$$

$$-L[\widetilde{(\rho w)^*_{top}q^*_{top}}n_z F_{top}-\widetilde{(\rho w^*_{bot}q^*_{bot}}n_z F_{bot}]$$

$$-L\int_V (q_c-q_E)dV. \qquad (6)$$

$\Delta p=p_{top}-p_{bot}$ is the pressure at the top minus pressure at the bottom of the volume. Finally, the left sides of eq (5) and (6) are solved under the assumption that the top and bottom of the respective layer volumes may move vertically in time.

Thus, we obtain the relation

$$\int_V \frac{\partial}{\partial t}\rho(c_v T+gz)dV=-\frac{1}{g}\int_F \frac{\partial}{\partial t}(\overline{c_v T}+\overline{gz})\Delta p dF$$

$$+\frac{1}{g}\int_{F_{top}}\frac{dp_{top}}{dt}(c_v T+gz)_{top}dF$$

$$-\frac{1}{g}\int_{F_{bot}}\frac{dp_{bot}}{dt}(c_v T+gz)_{bot}dF$$

$$=-\frac{1}{g}\frac{\partial}{\partial t}\widetilde{(c_v\overline{T}+\overline{gz})\Delta p}F$$

$$+\frac{1}{g}\frac{dp_{top}}{dt}(c_v T+gz)_{top}F_{top}$$

$$-\frac{1}{g}\frac{dp_{bot}}{dt}(c_v T+gz)_{bot}F_{bot} \qquad (7)$$

and

$$\int_V \frac{\partial}{\partial t}(\rho q)dV=-\frac{L}{g}\frac{\partial}{\partial t}\widetilde{q\Delta p}F+\frac{L}{g}\frac{dp_{top}}{dt}q_{top}F_{top}$$

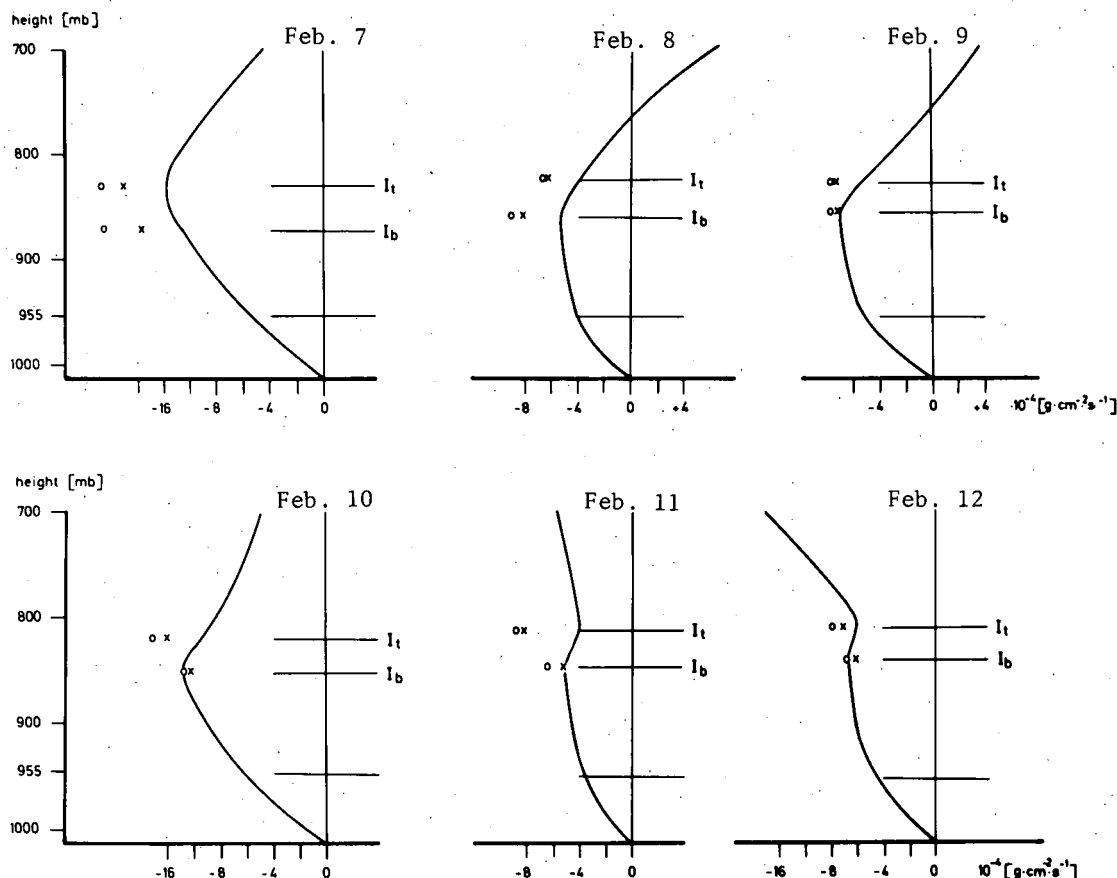$$-\frac{L}{g}\frac{dp_{bot}}{dt}q_{bot}F_{bot}. \qquad (8)$$

FIGURE 6.—Vertical mass transport averaged on each day for the center of the triangle. The crosses indicate the sum of vertical mass transport due to the vertical motion and the exchange between the layers above and below the inversion (due to the inversion slope in space). The open circles show the total mass transport through the inversion boundaries, including the effect of the vertical movement of the boundaries in time.

Combining eq (5) and (6) with (7) and (8), respectively, we can estimate the mean transports through the surface of the volume, and the local changes, after determining the mean vertical motion $\tilde{w}$. Mean vertical velocity was computed by the kinematic method.

The mass budget was computed by integration of the equation of continuity, assuming stationarity (i.e., $\partial\rho/\partial t = 0$). The turbulent, vertical, sensible, and latent heat fluxes are estimated as residuals from the combined eq (5) and (7) and (6) and (8), respectively. The turbulent fluxes at the sea surface were computed by the aerodynamic bulk formulas at each ship and averaged for the triangle. Simultaneous measurements of fluxes by the profile method at *Meteor* have shown that the difference of the daily averages of both values is less than 10 percent.

5. THE MASS TRANSPORT AND MEAN VERTICAL MOTION

In an early study, v. Ficker (1936) suggested that the trade-wind inversion is a layer that separates the air masses embedded in the flow above and below the inversion. Riehl et al. (1951) have clearly shown from measurements over the Pacific Ocean that, dynamically, this assumption cannot be accepted. On the contrary, these authors found that there is a net mass transport downward through the inversion. These results, however, were based on one-
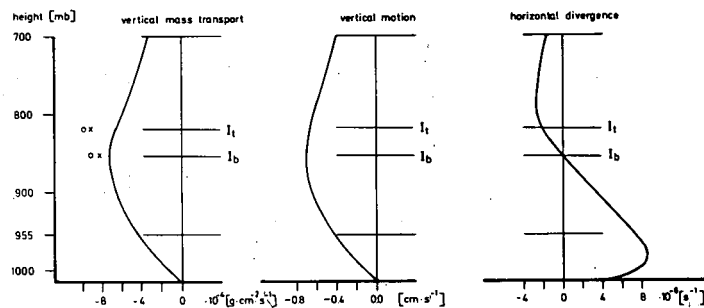

FIGURE 7.—Vertical mass transport, vertical motion, and horizontal divergence for the center of the triangle averaged over the period, Feb. 7–12, 1969.

dimensional divergence computations. The triangular ship arrangement during ATEX offered an opportunity to determine the vertical mass transport in the low-level trade-wind layer without serious restrictions. The results of the daily averaged mean downward mass transports are shown in figure 6. In this graph, the vertical subsidence and the mass flux through the boundary due to the slope effect and the height changes of the inversion are separated. On all days, the curves demonstrate that there is a downward mass transport through the whole regime with a maximum value at the inversion base, decreasing upward and downward. This result implies that the trade
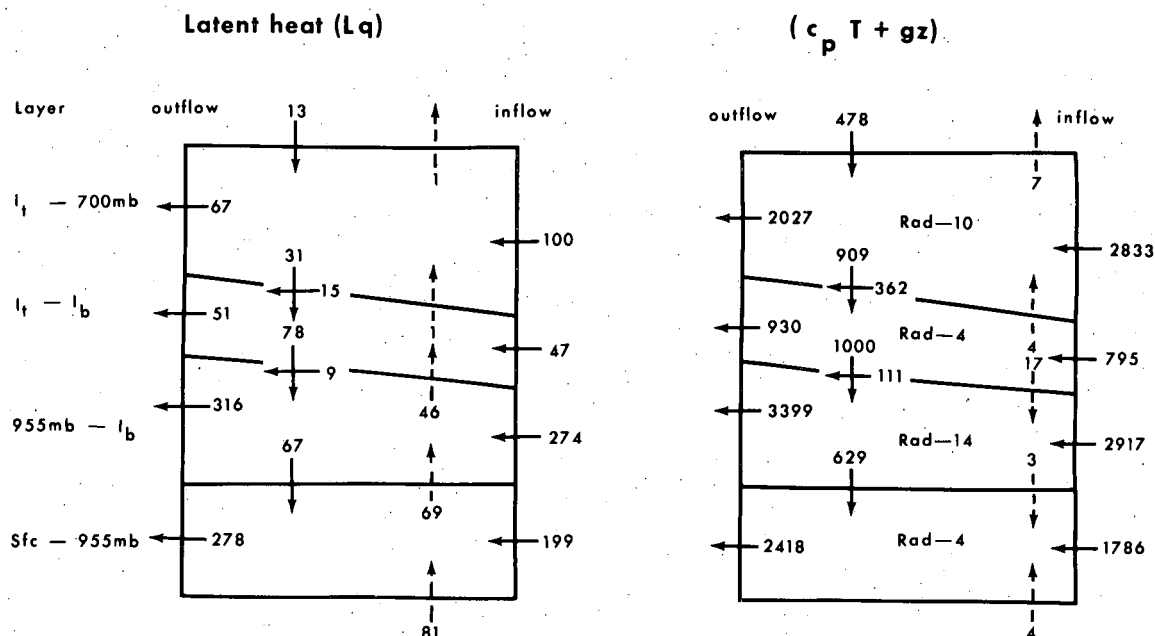
FIGURE 8.—Budgets of latent heat (10^{16} cal/day), and of enthalpy plus geopotential energy (10^{16} cal/day), for the subcloud layer, the cloud layer, the inversion layer, and the layer above the inversion up to 700 mb for the ATEX triangle, Feb. 7–12, 1969. Full arrows indicate transports by the mean motion; broken arrows, the residual turbulent fluxes. Radiation sink is indicated in the sensible heat budget; the net latent heat release is zero for the moisture budget.

inversion is not a solid layer but marks a region of an extremely strong, mean downward mass transport.

The general characteristics of vertical mass flux, vertical motion, and horizontal divergence are clearly reflected in the 6-day average profiles shown in figure 7. Obviously, the layer between the sea surface and the inversion base is governed by a remarkable horizontal divergence while the upper zone, between the inversion base and 700 mb, shows a slight convergence. The strongest horizontal divergence appears to be at approximately 985 mb, where the wind speed also has its maximum.

The coincidence between the inversion base and non-divergence seems to be systematic. Thus, air particles are vertically accelerated downward above and decelerated below the inversion base due to the mean vertical motion field. This is approximately true for every day as may be seen from figure 6.

The inversion height is variable in time, but this layer does not migrate progressively downward with the mean motion. It must, therefore, be balanced by an upward-directed process. As demonstrated by Ball (1960) using meteorological measurements and by Rouse and Dodu (1955) based on laboratory experiments, the most plausible process seems to be upward turbulent mixing leading to the establishment of the inversion base. Since this height generally coincides with the top of trade-wind cumuli, it is suggestive that mainly cumulus convection will achieve the required mixing (Riehl et al. 1951). This argument is reinforced by the water vapor and heat budget calculations presented in the following section. The total mass transport through the inversion boundaries is achieved not only by the large-scale vertical sinking but additionally by the vertical motion of the inversion itself and by its horizontal slope. As indicated in figure 7, these

effects increase the downward mass transport through this layer. During the analyzed period, about one-half of the mass within a column between sea surface and inversion base moving downstream was replaced daily by dry air masses from above. This fact is highly important for water vapor accumulation and cloud develpment in the lower layers.

6. THE HEAT BUDGET

The Total Budget

The heat budget estimates of the low-level ATEX column are based on the mass transport discussed in section 5 and on the temperature and humidity profiles measured at the corners of the triangle. The transports through the horizontal and vertical surfaces of the different layers averaged over the 6-day period are presented in figure 8. The subgrid-scale fluxes (dashed arrows) are determined as a residual in the budget equations for each horizontal surface of the four layers from the surface to the 700-mb level upward. The radiative cooling was estimated from computations using formulas of Rodgers and Walshaw (1966) for the long-wave component and those from Roach (1961) for the short-wave part. Although a rough correction for cloudiness is made, these values should be considered tentative. However, more precise calculations should not significantly change our results. The numbers, given in 10^{16} cal/day, refer to the surface of the triangular column with a mean base area of 2.2×10^{5} km². The calculated inflow and outflow values show that there is a horizontal divergence of energy below and a convergence above the inversion layer.
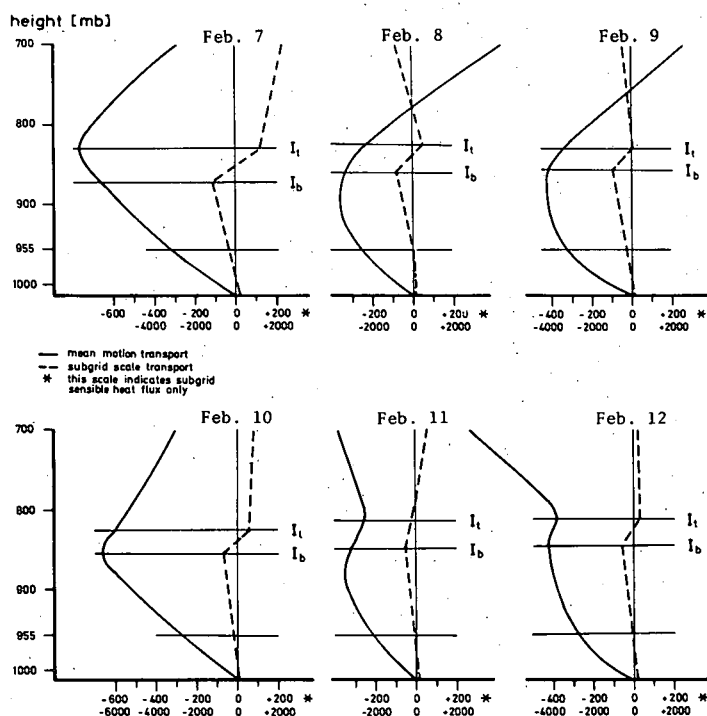
FIGURE 9.—Daily values of the vertical flux of enthalpy plus potential energy (ly/day), notation as in figure 8. The abscissa denoted by asterisks refers to subgrid-scale sensible heat fluxes.
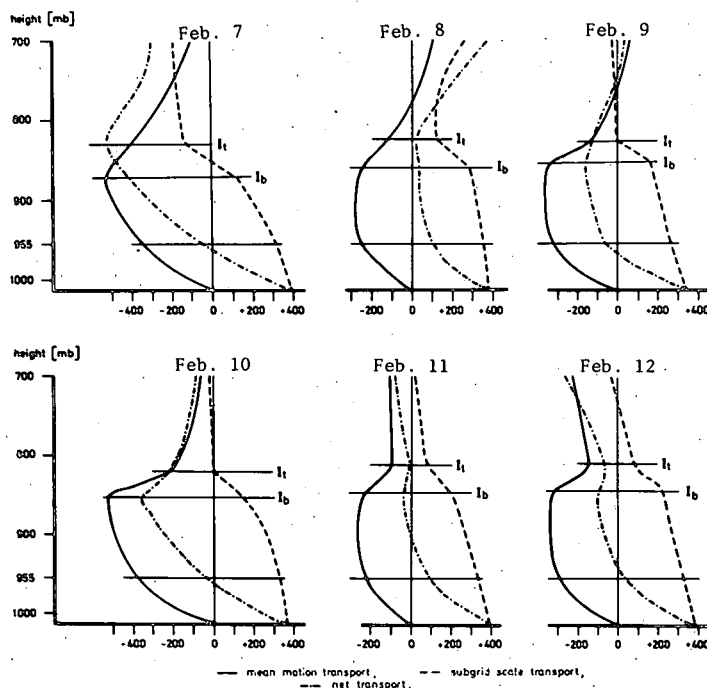

FIGURE 10.—Daily values of the vertical flux of latent heat (ly/day). The dash-dotted line represents the actual transport required for moisture balance.

Vertical Fluxes of Enthalpy and Geopotential Energy

The vertical transports of enthalpy and geopotential energy are portrayed in more detail in figure 9. The shape of the mean downward transport curve is generally governed by a maximum at the inversion. Thus, the low
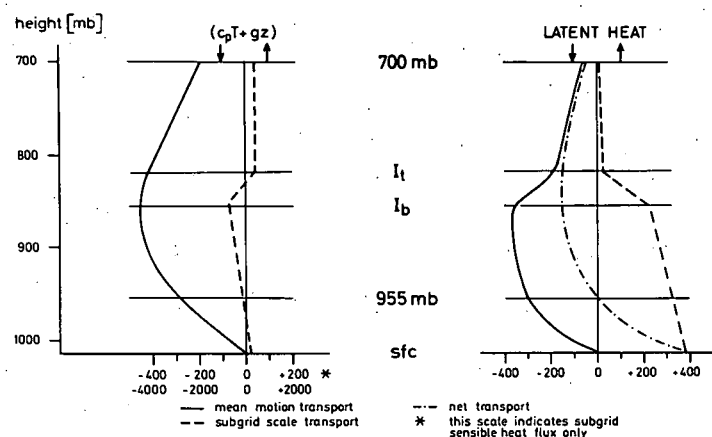

FIGURE 11.—Transports of enthalpy plus potential energy (ly/day), and of latent heat (ly/day), averaged for the period, Feb. 7–12, 1969. Notation as in figures 9 and 10.

troposphere does not receive the major portion of this energy component from the sea surface in any direct sense. Instead, there is an interplay of energy transformation and transport that finally results in the dry downward sinking of air mass in this part of the trades. Although this fact is of great importance to the physical processes in the lower atmosphere, it cannot be interpreted as a net input of energy into the atmosphere at all. Instead, we are observing only one scale of an interacting system. The primary energy source must be attributed to the large convective systems with strong cumulonimbi development, especially in the equatorial trough region. Gray (1971), among many others, recently stated the importance of the heating mechanism due to moist upflow and dry downflow of air.

The residual subgrid flux of sensible heat is a result of a small difference between large quantities. It, therefore, includes a degree of uncertainty. However, we believe that this result supports the conclusion that a balance of our computed (c_pT+gz) budget can be achieved, resulting in reasonable subgrid-scale fluxes.

Vertical Fluxes of Latent Heat

The daily averaged mean downward fluxes of latent heat in figure 10 display similar characteristics to those of (c_pT+gz); but, here, the subgrid-scale values are of the same order of magnitude as the mean transports. The evaporation rate at the sea surface nearly equals the downward water vapor transport due to mean motion at the inversion base. The graphs for the individual days are obviously in good agreement. Therefore, the dominant features will become particularly clear in the profiles averaged over the whole period (fig. 11).

With respect to the vertical latent heat transport, we find an interesting relation between the large-scale and the subgrid-scale fluxes. About 55 percent of the evaporated water at the sea surface is transported upward into the inversion layer by subgrid-scale processes. The rate of upward transport depends on an equilibrium between mean downward sinking and upward

turbulent mixing, which constantly reestablishes and determines the inversion base. Convergence of water vapor in the inversion layer is counteracted by the downward transport accomplished by mean subsiding air in opposition to the upward convective transport of the cloud elements. In fact, there is an additional net moisture input from above the inversion into the cloud layer. Thus, the total input of latent heat from the sea surface is accumulated in the cloud and subcloud layer and transported horizontally into the equatorial trough region.

The Horizontal Transports of Sensible and Latent Heat

The work by v. Ficker (1936), which is based on the *Meteor* observations obtained in 1925–27 and many other studies, indicates clearly that there is a substantial meridional transport of sensible heat, geopotential energy, and water vapor in the direction of the equatorial trough region in the whole trade-wind area. Those findings are supported by our measurements.

Figure 12A shows the downstream transports at the center of the ATEX triangle. The length of the thick horizontal lines indicates the flux magnitude per day across a vertical surface with a base line of 1 cm and the height of the layer. The strongest transports occur in the layer below the inversion. The percentage numbers indicate that portion of latent heat or enthalpy and geopotential energy which contributes to the total transport by horizontal divergence within a column with a length of 500 km. This distance is traversed by an air parcel in about one day. The minus sign means horizontal convergence; that is, the horizontally transported air loses energy. Evidently, the largest gain of energy in the trades is found in the subcloud layer. The layers above the inversion base lose energy downstream.

The zonal and meridional components of the transports, as seen in figure 12B, suggest a strong meridional flow toward the Equator in the lower layers where energy is accumulated, a small equatorward flow in the inversion layer, and a poleward flow above the inversion where energy is extracted. Under these conditions, therefore, a portion of the northwestward transported energy above the inversion moves downward and contributes again to the low-level flow. The region between the sea surface and the trade inversion under undisturbed conditions acts like a channel with a semipermeable top and bottom (with respect to energy) where large amounts of energy are accumulated and transported into the equatorial trough region.

Some Aspects of the Turbulent Flux Mechanisms

While the fluxes at the sea surface were measured or computed by the bulk aerodynamic formulas, the vertical distribution of subgrid-scale fluxes beyond that point could be determined only as a residual of the budget cal-
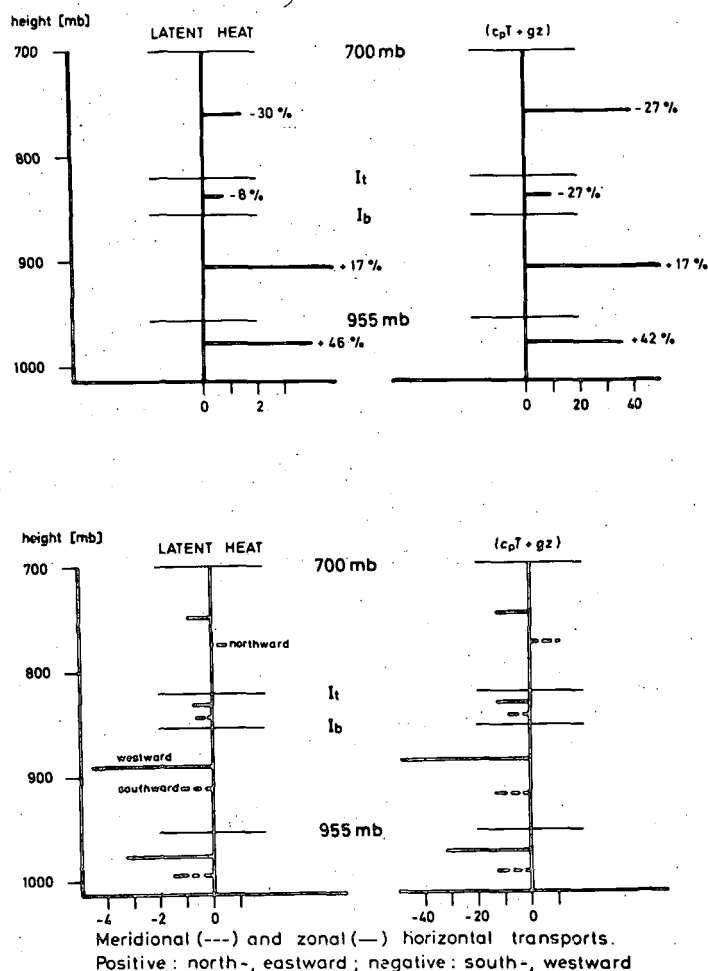

Meridional (---) and zonal (—) horizontal transports.
Positive : north-, eastward ; negative: south-, westward

FIGURE 12.—Horizontal, layer-integrated energy transport (10^{10} cal·day^{-1}·cm^{-1}): (A) total downstream transports across a surface with a base line of 1 cm and the height of the layer [percentages indicate the effects of horizontal divergence (+) or convergence (−) relative to the total transport when integrated over a steady-state trajectory of 500-km length] and (B) meridional and zonal transports (positive toward north and east).

culations. Information concerning the mechanisms achieving these transports was not obtained in ATEX, but some qualitative arguments can be offered from the temperature and specific humidity profiles.

In agreement with earlier studies, we find nearly constant potential temperature and small gradients of specific humidity in the layer between 100 and about 500 m. Therefore, microscale processes, as described by the austausch concept, can hardly be responsible for the vertical turbulent fluxes in this layer. This argument is furthermore supported by the fact that 35 percent of all soundings during ATEX have a constant or even an increasing specific humidity with height in that layer. Hence, organized processes such as dry convection must achieve the subgrid-scale upward transports in the subcloud layer as suggested by Garstang et al. (1970).

As far as the cloud layer is concerned, there is little doubt that cumulus convection is the governing mecha-

nism in the vertical transport of latent and sensible heat. The upward turbulent water vapor flux breaks down in the inversion, where cumulus convection terminates. This fact explains the considerable upward subgrid-scale transports of water vapor into the inversion as well as the strong decrease within the inversion layer. Cumulus convection penetrating the inversion base also permits the calculated downward transport of sensible heat to exist at the inversion base. Such downward transport may be accomplished by at least two processes. On the one hand, cloud air in the inversion is potentially colder than the sinking environmental air; on the other hand, liquid water evaporating in the inversion layer effectively represents downward transport of sensible heat.

A test should be conducted to determine whether or not the large upward turbulent transport of 68×10^{16} cal/day can be accomplished by the cumulus clouds in the convective layer just above cloud base.

The whole area $A = A_a + A_c + A_d$, where A_a is the area of actively ascending towers, A_c is stationary decaying cloud matter, and A_d is the clear area of compensatory descent. From climatic charts and ship observations during ATEX, we find that

$$A_d = A_a + A_c. \tag{7}$$

The upward flux of water vapor by turbulent motions, F_q, is given by

$$F_q = (\rho_{wa} w_a A_a + \rho_{wd} w_d A_d)L \tag{8}$$

if $w=0$ in the area A_c, L is the latent heat of vaporization, w_a is the rate of ascent in the towers, ρ_{wa} and ρ_{wd} are the water vapor densities of the upward- and downward-moving air masses, respectively, and w_d is the rate of descent in the clear area. Since $q = \rho_w/\rho$, eq (8) becomes

$$F_q = \rho(q_a w_a A_a + q_d w_d A_d)L. \tag{9}$$

Here, it is assumed with little error that $\rho_a = \rho_d = \rho$, which follows from $T_a = T_d$ as demonstrated by many aircraft traverses through small cumuli. The equation of mass continuity is given by

$$w_a A_a + w_d A_d = 0 \tag{10}$$

where w_d is additional to the downward mean mass flow discussed earlier. Combining eq (10) and (9), we get

$$F_q = -\rho w_d A_d (q_a - q_d)L$$

or

$$-w_d = \frac{F_q}{\rho A_d(q_a - q_d)L}. \tag{11}$$

By inserting the numbers $F_q = 68 \times 10^{11}$ cal/s, $\rho = 1.1 \times 10^{-3}$ g·cm^{-3}, $A_d = 10^{15}$ cm^2, $L = 600$ cal/g and $q_a - q_d = 2.5$ g/kg, where q_d is the mean specific humidity of the soundings and q_a is the saturation specific humidity at the average temperature, we find that $w_d = -4$ cm/s. This is larger than that obtained by Riehl et al. (1951) because in our case $q_a - q_d$ is much smaller. Nevertheless, the value falls entirely within the reasonable range.

We now wish to compute A_a, given a reasonable estimate of w_a, to see if only a small fraction of the whole area is covered by actively rising towers as oberved. Using time-lapse photographs, we estimated w_a to be 1 m/s for trade-wind cumuli. With this value,

$$\frac{A_a}{A} = -\frac{w_d}{w_a}\frac{A_d}{A} = 0.02$$

a very small fraction indeed. We see, therefore, that the normal trade-wind atmosphere can indeed easily produce the transport of water vapor required by our budget calculation. These findings support those of Riehl et al. (1951).

7. CONCLUSIONS

The measurements during ATEX have shown that, under well-developed trade-wind conditions with little convective activity, the trade-wind inversion separates a low-level horizontal divergent layer from a convergent regime above. The maximum divergence tends to coincide with the maximum wind speed near the 400-m height. Using an average of 6 days, we found downward motion over the height range between the sea surface and the 700-mb level over the whole region. Maximum downward motion of about 600 m/day is found at the inversion base. Thus, the inversion is not a solid barrier to the vertical mass and energy transports; it is instead a region of maximum downward fluxes due to mean motion. On the other hand, there is a remarkable vertical subgrid-scale flux of moisture in the layer between the sea surface and the inversion. The turbulent water vapor fluxes into the inversion from below are relatively strong, but they are suppressed in the inversion layer and become nearly zero at its top. This flux convergence counteracts the drying effect of the mean downward motion and preserves the strong humidity gradient in the inversion layer. Furthermore, the combination of mean downward and turbulent upward water vapor flux in the lower layers ensures that the total latent heat input from the sea surface is, in fact, accumulated and transported downstream in the trade-wind flow below the inversion. The warm dry air from above, with its capability to absorb large quantities of water vapor, prevents condensation in the low-level trade-wind air and, therefore, guarantees that a large amount of latent heat is transported from the trade-wind areas into the equatorial trough region.

The upward latent heat flux and the downward sensible heat flux at the inversion base support the contention that cumulus convection is the predominant means of turbulent transfer at this level. Under these undisturbed conditions, the kinematic field and the static structure of the layer below the inversion are marked by only small time and space variations, in contrast to the layer above the inversion.

REFERENCES

Augstein, Ernst, "Mass and Heat Budget Estimations of the Atlantic SE Trade Wind Flow at the Equator," *Meteor-Forschungsergebnisse*, Ser. B, No. 8, Borntrager Verlag, Berlin, Germany, **1972**, pp. 31–41.

Augstein, Ernst, Hoeber, H., and Krügermeyer, L., "Fehler bei Temperatur-, Feuchte- und Windmessungen auf Schiffen in tropischen Breiten," *Meteor-Forschungsergebnisse*, Ser. B, No. 9, Borntrager Verlag, Berlin, Germany, **1973** (in press).

Aspliden, C. I., "On Energy Distribution in the Tropical Troposphere," *Dissertation*, Florida State University, Tallahassee, **1971**, 232 pp.

Ball, F. K., "Control of Inversion Height by Surface Heating," *Quarterly Journal of the Royal Meteorological Society*, Vol. 86, No. 370, London, England, Oct. **1960**, pp. 483–494.

Brocks, Karl, "Die Atlantische Expedition 1969 (GARP) mit dem Atlantischen Passat Experiment (APEX)," *Meteor-Forschungsergebnisse*, Ser. A, No. 9, **1972**.

Brümmer, Burghard, Ostapoff, F., and Schmidt, H., "The Aerological Measurements During ATEX," *NOAA Technical Report* **1973** (in press).

Bunker, Andrew F., Haurwitz, B., Malkus, J. S., and Stommel, H., "Vertical Distribution of Temperature and Humidity Over the Caribbean Sea," *papers in Physical Oceanography and Meteorology*, Massachusetts Institute of Technology and Woods Hole Oceanographic Institution, Vol. 11, Mass., **1950**, pp. 1–82.

Ficker, H. v., "Bemerkungen über den Wärmeumstaz innerhalb der Passatzirkulation," Verlag Akademische Wissenschaften, Berlin, Germany, **1936**.

Garstang, Michael, La Seur, Noel E., Hadlock, R., "Results From a Comprehensive Tropical Field Experiment," *Proceedings of the International Conference on Tropical Meteorology, June 2–11, 1970,* University of Hawaii, Hawaii, **1970**, pp. 1–7.

Garstang, Michael, "A Review of Hurricane and Tropical Meteorology," *Bulletin of the American Meteorological Society*, Vol. 53, No. 7, July **1972**, pp. 612–630.

Gray, William M., "The Magnitude of and the Fundamental Role of the Up-moist and Down-dry Vertical Circulation of the Troposphere," paper presented at the VII Technical Conference on Hurricanes and Tropical Meteorology, *December 6–9, 1971,* Barbados, West Indies, **1971**.

Malkus, Joanne, S., "On the Structure of the Trade Wind Moist Layer," *papers in Physical Oceanography and Meteorology,* Massachusetts Institute of Technology and Woods Hole Oceanographic Institution, Vol. 13, No. 2, **1958**, pp. 1–48.

Riehl, Herbert, Yeh, C., Malkus, Joanne S., and La Seur, Noel E., "The North-east Trade of the Pacific Ocean," *Quarterly Journal of the Royal Meteorological Society*, Vol. 77, No. 334, London, England, Oct. **1951**, pp. 598–626.

Riehl, Herbert, and Malkus, Joanne S., "On the Heat Balance and Maintenance of the Circulation in the Trades," *Quarterly Journal of the Royal Meteorological Society*, Vol. 83, No. 355, London, England, Jan. **1957**, pp. 21–29.

Riehl, Herbert, and Malkus, Joanne S., "On the Heat Balance of the Equatorial Trough Zone," *Geophysica,* Vol. 6, No. 3/4, Helsinki, Finland, **1958**, pp. 503–538.

Roach, W. T., "The Absorption of Radiation by Water Vapor and Carbon Dioxide in a Cloudless Atmosphere," *Quarterly Journal of the Royal Meteorological Society*, Vol. 87, No. 373, London, England, July **1961**, pp. 364–373.

Rodgers, C. D., Walshaw, S. D., "The Computation of Infrared Cooling Rate in Planetary Atmospheres," *Quarterly Journal of of the Royal Meteorological Society*, Vol. 92, No. 391, London, England, Jan. **1966**, pp. 67–92.

Rouse, H., and Dodu, J., "Turbulent Diffusion Across a Density Discontinuity," *La Houille Blanche*, Vol. 10, No. 4, **1955**, pp. 522–532.

Soltwisch, D., "Die symoptische Wetterlage über dem tropischen Nordatlantik wahrend der Atlantischen Passat Experimente (ATEX/APEX) in Februar 1969 und Zusammenhänge zwischen grobraumigen Vorgängen und dynamischen Prozessen der planetarischen Grenzschicht," Thesis, Fachbereich Geowissenschaften, Freie Universitat Berlin, Germany, **1973** (in preparation).